Critical coupling for dynamical chiral-symmetry breaking

Craig D. Roberts* and Bruce H. J. McKellar
Research Centre for High Energy Physics, School of Physics, The University of Melbourne, Parkville, Victoria 3052, Australia
(Received 1 August 1989)

We study chiral-symmetry breaking in a model of quantum chromodynamics (QCD). In our study we make a critical analysis of an approximation that is often used in QCD and other theories to simplify the Schwinger-Dyson equation for the fermion self-energy. Solving the Schwinger-Dyson equation numerically, without employing the approximation, we find that chiral symmetry is restored when the running coupling constant at zero momentum transfer falls below 0.890.

I. INTRODUCTION

The possibility of dynamical chiral-symmetry breaking (DCSB) is an important consideration in many theories. In QCD one can understand the small value of the pion-to-proton mass ratio and the success of the current algebra and PCAC (partial conservation of axial-vector current) formalism if one assumes DCSB. In extended technicolor theories DCSB is also important for there the nonzero value of the bilinear technifermion condensate entailed by the assumption of DCSB leads to nonzero quark and lepton masses. These results are significant and provide a compelling reason to study the phenomenon of DCSB itself in detail and to try and determine which aspects of a given theory are responsible for the dynamical breakdown of chiral symmetry.

The most obvious means of studying chiral-symmetry breaking is to use the Schwinger-Dyson equation whose solution is the propagator (S) (or self-energy Σ) for a fermion in the given theory. This is because $\mathrm{tr}S \propto \langle \bar{\psi}\psi \rangle$, the bilinear fermion condensate, and so one is able to study the condensate (a nonzero value of which signals DCSB) directly once the equation has been solved. The problem with this approach, stated here using the terminology of QCD but relevant generally, is that the Schwinger-Dyson equation involves the exact gluon propagator and also the exact quark-gluon vertex, each of which can be calculated only by solving other Schwinger-Dyson-type equations. The equation for the quark self-energy is therefore not a closed equation and presently any tractable study of DCSB using this method necessarily requires that some approximations and truncations be made.

In QCD (on which we shall now concentrate) an often used approximation is to write the (Landau gauge) gluon propagator in the form[1]

$$g^2 D^{\mu\nu}(q) = 4\pi \frac{\alpha(-q^2/\Lambda^2)}{q^2}\left[-g^{\mu\nu}+\frac{q^\mu q^\nu}{q^2}\right],$$

where $\alpha(-q^2/\Lambda^2)$ is the QCD running coupling constant. This would be an exact result if there were no ghost contributions but in Landau-gauge QCD it is an approximation. The QCD running coupling is calculable for $-q^2 \gg \Lambda^2$ but in the infrared and intermediate momentum-transfer regimes it is not. One cannot proceed to solve the equation therefore until some ansatz is made for the running coupling at these smaller momentum transfers. For our purpose we choose here[2]

$$\alpha\left[-\frac{q^2}{\Lambda^2}\right] = \frac{\lambda\pi}{\ln\left[1+\epsilon+\frac{-q^2}{\Lambda^2}\right]} \tag{1.1}$$

with $\lambda = 12/(33-2N_F)$, which is obviously just a simple extension of the form used with success to fit the spectroscopic data of the ψ and γ systems in Ref. 3.

It is also necessary to make some ansatz for the connected quark-gluon vertex $\Gamma^\mu(p,q)$. Gauge invariance in QCD requires that Γ^μ satisfy a Slavnov-Taylor identity. Neglecting ghost contributions (as we did for the gluon propagator) this identity reads

$$(p-q)_\mu \Gamma^\mu(p,q) = S^{-1}(p) - S^{-1}(q) . \tag{1.2}$$

This constrains the longitudinal part of the vertex. Writing

$$S^{-1}(q) = \not{q} A(q^2) - B(q^2) \tag{1.3}$$

it is easy to see that a solution of this identity is[4]

$$\Gamma^\mu(p,q) = \text{transverse part} + A(p^2)\gamma^\mu + \frac{k^\mu}{k^2}\{[A(p^2)-A(q^2)]\not{q} - [B(p^2)-B(q^2)]\} \tag{1.4}$$

(with $k=p-q$). This is not a solution of the vertex equation (as can be seen by direct substitution) but it does represent an improvement over simply using the bare vertex. Assuming that the "transverse part" in Eq. (1.4) vanishes in the Landau gauge then

$$D^{\mu\nu}(p-q)\Gamma_\nu(q,p) = D^{\mu\nu}(p-q)A(q^2)\gamma_\nu . \tag{1.5}$$

Using Eqs. (1.1) and (1.5) we obtain the following closed, approximate Schwinger-Dyson equation in QCD:

$$[A(p^2)-1]\not{p}-B(p^2)=\frac{4}{3}i\int\frac{d^4q}{(2\pi)^4}g^2D^{\mu\nu}(p-q)\gamma_\mu \times\frac{A(q^2)}{A(q^2)\not{q}-B(q^2)}\gamma_\nu . \tag{1.6}$$

We remark that this is also the vacuum field equation that arises in a global color-symmetry model[5] of QCD. In this connection its role in DCSB is even more transparent because the general solution of this equation describes a set of degenerate physical vacua, each element of which represents a distinct, admissible vacuum state. Only one of the states can be physically realized, however, leading to a situation where the vacuum state does not have the symmetry of the Lagrangian and consequently the appearance of Goldstone bosons.

In this paper we search for a chiral-symmetry phase transition in QCD using Eq. (1.6). This problem is addressed in Ref. 6 but therein, after Wick rotation to Euclidean metric, the angular integral in Eq. (1.6) is approximated and the integral equation converted into a differential equation. We show how this approximation affects the solution of the Schwinger-Dyson equation and discuss whether the conclusions that one draws when employing it can be trusted. The relevance of our analysis extends beyond the immediate problem of a chiral phase transition that we address here because this approximation has been used widely in studies of QCD (Refs. 1, 4, 6, and 7). It has also been employed in the study of quark and lepton mass generation in extended technicolor models.[8]

In Sec. II we discuss the approximation of the kernel in Eq. (1.6) and its implications in detail, comparing the approximated kernel with the exact kernel numerically to explicitly reveal the differences. We use the approximation to simplify the kernel in the integral equations and solve the resulting equations in Sec. III. The result should agree with the solution of the differential equation that can be derived from these approximated equations, so we also solve this differential equation numerically. Comparing the results provides a check on our integral equation code. In Sec. III we also present the solution obtained from the exact integral equations: i.e., without approximating the kernel. We summarize and discuss our results in Sec. IV.

II. COMPARSION OF THE EXACT AND APPROXIMATE KERNELS

After a Wick rotation to Euclidean metric, Eq. (1.6) yields the following pair of nonlinear, coupled integral equations for the quark wave-function renormalization and self-mass function:

$$[A(p^2)-1]p^2=\frac{16\pi}{3}\int\frac{d^4q}{(2\pi)^4}\frac{\alpha((p-q)^2/\Lambda^2)}{(p-q)^2} \times\left[p\cdot q+2\frac{p\cdot(p-q)q\cdot(p-q)}{(p-q)^2}\right] \times\frac{A^2(q^2)}{A^2(q^2)q^2+B^2(q^2)}, \tag{2.1}$$

$$B(p^2)=16\pi\int\frac{d^4q}{(2\pi)^4}\frac{\alpha((p-q)^2/\Lambda^2)}{(p-q)^2} \times\frac{A(q^2)B(q^2)}{A^2(q^2)q^2+B^2(q^2)} . \tag{2.2}$$

It is clear that, when the angular integrals are evaluated, these equations reduce to one-dimensional integral equations over the magnitude-of-momentum variable. The kernel in Eq. (2.1) is

$$K_A(p,q)=\int d\Omega\frac{\alpha((p-q)^2/\Lambda^2)}{(p-q)^2} \times\left[p\cdot q+2\frac{p\cdot(p-q)q\cdot(p-q)}{(p-q)^2}\right], \tag{2.3}$$

where

$$\int d\Omega=\left[\int_0^\pi d\omega\sin^2\omega\int_0^\pi d\theta\sin\theta\int_0^{2\pi}d\phi\right]$$

and the kernel in Eq. (2.2) is

$$K_B(p,q)=\int d\Omega\frac{\alpha((p-q)^2/\Lambda^2)}{(p-q)^2} . \tag{2.4}$$

It is not difficult to establish that when $\alpha(q^2)=\hat{\alpha}$ (a constant)

$$K_A(p,q)\equiv 0 \tag{2.5}$$

and

$$K_B(p,q)=2\pi^2\hat{\alpha}\left[\theta(p^2-q^2)\frac{1}{p^2}+\theta(q^2-p^2)\frac{1}{q^2}\right], \tag{2.6}$$

which yields $A(p^2)\equiv 1$ as the solution of Eq. (2.1) and a single nonlinear integral equation for $B(p^2)$: Eq. (2.2) with $A(q^2)\equiv 1$. This is the situation in QED (Ref. 9) when fermion loops are not included in the photon polarization tensor.

The approximation that is usually made in models such as the one we are considering here is to assume that for $\alpha(q^2)\neq$const Eq. (2.5) is still correct and that Eq. (2.6) is modified only by the replacement

$$\hat{\alpha}\rightarrow\theta(p^2-q^2)\alpha(p^2/\Lambda^2)+\theta(q^2-p^2)\alpha(q^2/\Lambda^2) \tag{2.7}$$

[with the understanding that $\theta(a-b)\theta(b-a)\equiv 0$]. In Figs. 1 and 2 we plot the function

$$f(u,v)=K^{\text{exact}}(u,v)-K^{\text{approx}}(u,v) , \tag{2.8}$$

with $u=p/\Lambda$ and $v=q/\Lambda$, for the kernel of the A and B equations, respectively, with $\epsilon=1.0,2.0$, $N_F=0$, and $u=1$. The figures illustrate how the approximation underestimates the kernel for $p\simeq q$. One observes that the peak value of $f(u,v)$ increases with $[\alpha(0)-\alpha(\infty)]$ as does the domain on which the function is nonzero. This demonstrates that, assuming a monotonically decreasing running coupling, the approximation is most reliable when $[\alpha(0)-\alpha(\infty)]\sim 0$: so, for an asymptotically free theory $[\alpha(\infty)=0]$ the approximation is valid only if $\alpha(0)\sim 0$.

In the present model, with the coupling defined in Eq. (1.1), this approximation enables one to derive the follow-

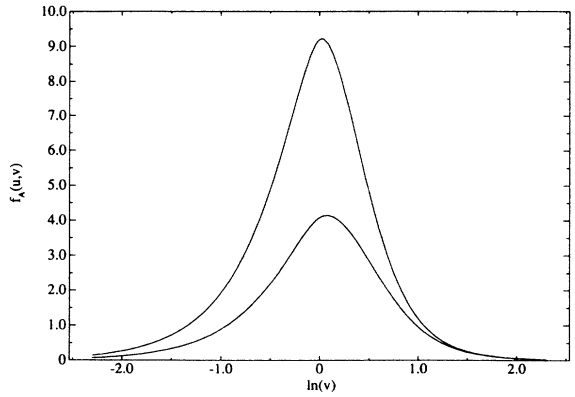

FIG. 1. The function in Eq. (2.8) is plotted for the kernel of Eq. (2.1) with $u=1$ and $N_F=0$. The tallest peak is obtained with $\epsilon=1.0$ while the other is the result with $\epsilon=2$.

ing differential equation for $b(x)=B(\Lambda^2 x)/\Lambda$:

$$0=b''(x)+\beta(x)b'(x)+\lambda\gamma(x)\frac{b(x)}{x+b^2(x)}\ , \tag{2.9}$$

with

$$\beta(x)=\frac{2x^2+x(x+2\xi)\ln\xi+2\xi^2(\ln\xi)^2}{x\xi\ln\xi(x+\xi\ln\xi)}$$

and

$$\gamma(x)=\frac{x+\xi\ln\xi}{x\xi(\ln\xi)^2}\ ,$$

where $\xi=\tau+x$ and $\tau=1+\epsilon$. This differential equation is equivalent to Eq. (2.2) with the approximated kernel provided the following boundary conditions are applied:

$$b'(0)=-\frac{\lambda}{2b(0)\ln\tau}\quad\text{and}\quad b(\infty)=0\ . \tag{2.10}$$

The complexity of this differential equation (DE) means that a complete solution can only be obtained numerically; however, it is not too difficult to show that, in the ultraviolet asymptotic regime,

$$b(x)|_{x\sim\infty}\to\frac{-4\pi^2\lambda}{3}\frac{\kappa}{x(\ln x)^{1-\lambda}} \tag{2.11}$$

with $\kappa=(\ln\mu^2)^{-\lambda}\langle\bar{q}q\rangle_\mu$, a renormalization point invariant. The constants here are not fixed by analysis of the asymptotic behavior of the DE but rather by matching the asymptotic form to the operator-product-expansion result.[10]

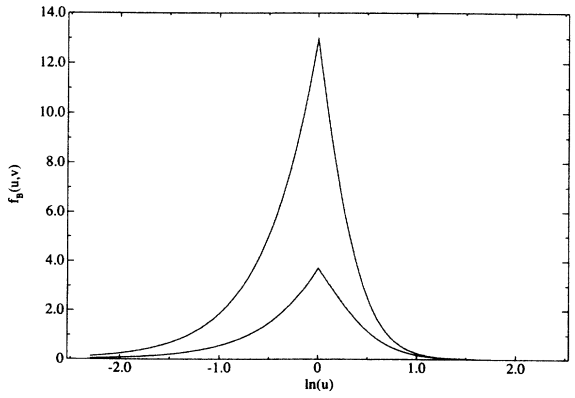

FIG. 2. The function in Eq. (2.8) is plotted here for the kernel of Eq. (2.2), again with $u=1$ and $N_F=0$. The tallest peak is again obtained with the smaller value of $\epsilon=1.0$ with the other curve being the result for $\epsilon=2.0$.

III. SOLUTION OF THE INTEGRAL EQUATIONS

We have solved Eqs. (2.1) and (2.2) using the approximations of Eqs. (2.5)–(2.7) for $N_F=0,4$ and a large range of values for τ $(=1+\epsilon)$ searching, of course, for a critical value of $\alpha=\alpha_c$ below which $\langle\bar{q}q\rangle=0$. In this case the kernel has a simple analytic form and so it is necessary to discretize only the solution functions. To solve the equations we employed a simple iterative procedure whereby an initial guess was made for the solution, $(A_0(p),B_0(p))$, on a discretized momentum grid in the domain $[0,1000\Lambda]$ (chosen so that the solution obtained was independent of the cutoff). This guess was substituted into the integrands of the integral equations and provided an iterate $(A_1(p),B_1(p))$ upon evaluating the integral. This iterate was then resubstituted to provide another iterate $(A_2(p),B_2(p))$. Writing F for A or B, then, at each p element of the grid, the next guess was determined as follows: if

$$\frac{|c_1(p)|}{|c_0(p)|}<1\ ,$$

with $c_0(p)=F_0(p)-F_1(p)$ and $c_1(p)=F_1(p)-F_2(p)$, then a geometric progression was fitted to the first three iterates and the next guess $F_0'(p)$ was taken to be

$$F_0'(p)=F_0(p)-\frac{c_0^2(p)}{c_0(p)-c_1(p)}\ ;$$

otherwise the next guess was taken to be

$$F_0'(p)=\frac{F_1(p)+F_2(p)}{2}\ .$$

This procedure was repeated until

$$\sup_p\left\{\frac{|A_0(p)-A_1(p)|}{A_0(p)},\frac{|B_0(p)-B_1(p)|}{B_0(p)}\right\}<10^{-3}\ ,$$

when the solution was accepted to be $(A_1(p),B_1(p))$.

We found, as one might expect, that for $\tau\ll\tau_c$ the procedure converged rapidly to a stable solution with $A(p^2)\equiv1$, $B(p^2)\not\equiv0$ [with UV asymptotic behavior matching Eq. (2.11)] and $\langle\bar{q}q\rangle\neq0$. As we increased τ, however, the procedure took longer to converge to a solution and it became important to ensure that many grid points were placed in the domain $[0,\Lambda]$. We settled on the criterion that a solution was only accepted if, to five significant figures, $B(p^2)$ was constant over the first 15 grid points so that we could be sure the grid spacing was

not relevant to the solution. In each series of runs, characterized by a particular value of N_F, there was always a value τ_b above which this criterion could no longer be satisfied. This determined when we discontinued a particular series. The value of τ_b could be increased by placing a finer grid mesh in the domain $[0,\Lambda]$, a procedure that could be continued until the point separation reached machine precision. In our calculations[11] this meant that we obtained the largest value of τ_b when the first nonzero grid point was $10^{-12}\Lambda$, there were 42 points in $[0,10^{-7}\Lambda]$ and 86 points in $[0,\Lambda]$ out of a total 136 points set in $[0,1000\Lambda]$. All of the results reported herein were obtained using this grid.

Two measures of DCSB are $B(0)\neq 0$ and the renormalization point invariant $\kappa\neq 0$ and in our analysis we have concentrated on these two *order parameters*. The results of our calculations are summarized in Figs. 3 and 4 where we have plotted $-1/\ln[B(0)]$ and $-1/\ln\kappa$ as functions of $\alpha(0)$ for $N_F=0,4$, respectively. In each case we have plotted the last data points calculated before the limit of numerical precision was reached. To the first, third, and fifth data points (measured in order of increasing α) we fitted a function

$$h(\alpha)=\beta(\alpha-\alpha_c)^{\gamma}\ , \tag{3.1}$$

with β, α_c, and γ the fitting parameters. The values we obtained for these parameters are presented in Table I. It is clear from the plots that this curve is a good representation of the data for $\alpha\simeq\alpha_c$. Such a function is familiar from the study of phase transitions in statistical mechanics. Using this analogy we identify γ as the critical exponent and α_c as the critical coupling associated with our two *order parameters* $-1/\ln B(0)$ and $-1/\ln\kappa$, zero values of which signify a restoration of chiral symmetry. From the table we estimate that

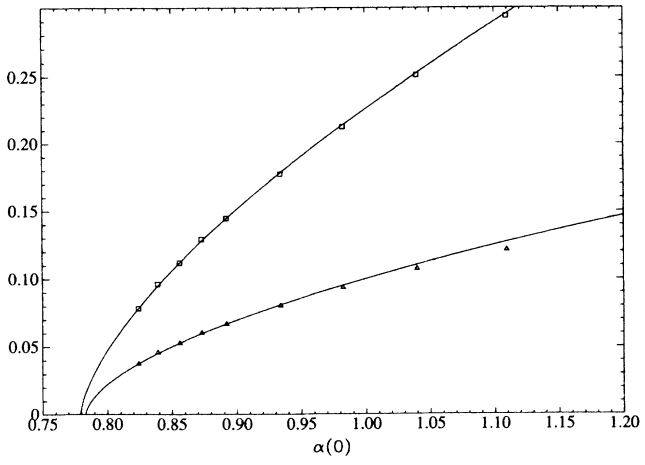

FIG. 3. The results obtained by solving Eq. (2.2) with the *approximate* kernel. □ mark the data points for $-1/\ln B(0)$ and △ mark the data points for $-1/\ln\kappa$. The smooth curves through the points show the fitting function of Eq. (3.1) with the parameter values described in the text. These results are for $N_F=0$.

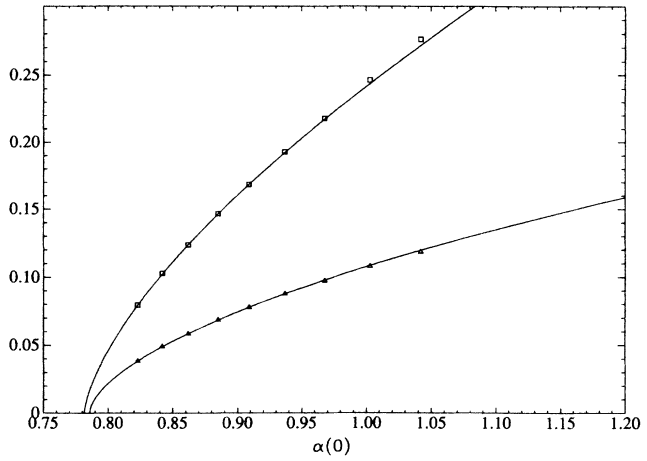

FIG. 4. Same as Fig. 3 but with $N_F=4$.

$$\gamma_{-1/\ln B(0)}=0.642\pm 0.036\ ,$$

$$\gamma_{-1/\ln\kappa}=0.587\pm 0.004\ ,$$

and

$$\alpha_c(0)=0.782\pm 0.003\ .$$

This means that chiral symmetry would be manifest in the model if $\alpha(0)$ was less than this value.

This result was obtained using the approximations of Eqs. (2.5)–(2.7) and we are interested in whether it depends in any way on these approximations. We will address this question shortly. However, before proceeding, we remark that the value of the critical coupling we have obtained differs from that reported in Ref. 6 where the differential equation of Eq. (2.9) is studied (although in a different form). (Qualitatively, we are in agreement: when the kernel is approximated there is a critical coupling below which chiral symmetry is restored.) The criterion that we have adopted as signifying chiral-symmetry restoration (the zero of the functions plotted in Figs. 3 and 4) is different to that adopted in Ref. 6 wherein chiral symmetry is assumed to be restored when the solution procedure used to solve the DE breaks down. This is analogous to our supposing that chiral symmetry is restored at τ_b.

TABLE I. Parameters obtained in fitting the function in Eq. (3.1) to the data presented in Figs. 3 and 4 obtained with the approximated kernel.

		β	α_c	γ
$N_F=0$	$-\frac{1}{\ln B(0)}$	0.617	0.779	0.664
	$-\frac{1}{\ln\kappa}$	0.245	0.783	0.584
$N_F=4$	$-\frac{1}{\ln B(0)}$	0.667	0.782	0.668
	$-\frac{1}{\ln\kappa}$	0.267	0.786	0.590

To check our results, i.e., to confirm that our solution procedure for the integral equation yielded correct results, we solved the DE in Eq. (2.9) numerically using fourth- and fifth-order Rünge-Kutta procedures. To solve this DE it is necessary to know the value of the solution function at some large finite value of x along with the first derivative of the function at that point. It is then a simple matter to integrate the DE in to $x=0$. The function we had obtained by directly solving the integral equation provided both the function value and an estimate of the first derivative of the function at all points $x\in[0,1000]$. To confirm this function as the correct solution we took the value of the function $x=950$ along with the estimate of its first derivative and used these quantities as the ultraviolet input for the DE.

We integrated the DE in to $x=0$ to obtain the solution of the differential equation, varying the value of the first derivative of the function (which we could only estimate from our numerical solution of the integral equation) until the solution function satisfied the infrared boundary condition of Eq. (2.10). We found that there was always a value of the first derivative at the ultraviolet boundary for which the infrared boundary condition could be satisfied and that as the mesh spacing was decreased the DE solution approached that returned by our integral equation code; i.e., $B^{\rm de}(p)\to B^{\rm ie}(p)\ \forall p$. This result confirmed that our integral equation solution procedure was indeed working correctly.

In solving the DE we observed that for large values of $\alpha(0)$ agreement between the two solutions was obtained with a relatively coarse mesh but as $\alpha(0)$ was decreased the mesh had to be made finer if the DE solution was to agree with the solution obtained from the integral equation. (If the mesh was too coarse the DE solution was too large at each p.)

Taking the integral equation solution now as the correct solution function we see that numerically solving the DE only yields the correct solution if the grid is made progressively finer as $\alpha(0)$ is decreased. Obviously, again, a machine precision problem arises in this approach but the projection technique could be used to determine the critical coupling nevertheless. The fact that such a projection technique was not used in Ref. 6 may be the cause of the discrepancy between our results and theirs. The fact that our DE solution agreed with our integral equation solution for a large range of τ values makes us confident of our results.

We now present the results obtained by solving Eqs. (2.1) and (2.2) with the kernel evaluated exactly; that is, without approximating the angular integrals in Eqs. (2.3) and (2.4). In this case we broke the kernel into two parts:

$$K(u,v)=K^{\rm approx}(u,v)+f(u,v)$$

with $K^{\rm approx}(u,v)$ defined in Eqs. (2.5)–(2.7) and $f(u,v)$ defined in Eq. (2.8). In solving the equations we calculated $f(u,v)$ on a $(nu=131\times nv=261)$ point grid with one v point placed at each u point and one placed between each pair of u points. When evaluating the integrals we interpolated this correction function off the grid using a cubic spline. Apart from this difference the solution procedure was exactly the same as discussed above in connection with the approximated kernel.

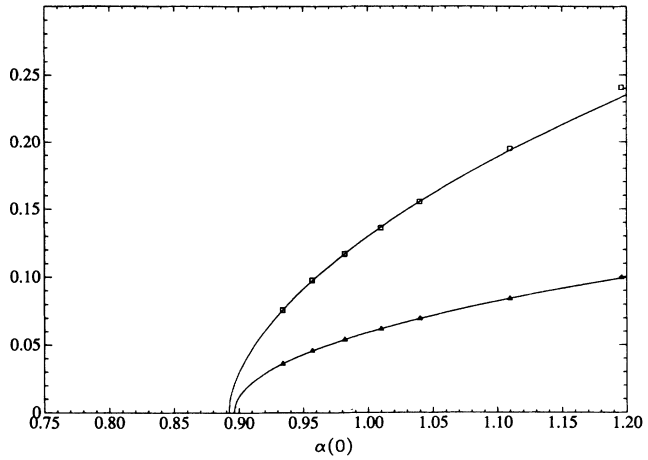

FIG. 5. The results obtained by solving Eq. (2.2) with the *exact* kernel. Again □ mark the data for $-1/\ln B(0)$ and △ the data for $-1/\ln\kappa$ with the smooth curves being the fitting function of Eq. (3.1) with the parameter values given in the text. These results are for $N_F=0$.

Our results are presented in Figs. 5 and 6. The values of the fitting parameters obtained through fitting Eq. (3.1) to the data are presented in Table II. From the table we estimate that

$$\gamma_{-1/\ln B(0)}=0.589\pm0.031\ ,$$

$$\gamma_{-1/\ln\kappa}=0.513\pm0.038\ ,$$

and

$$\alpha_c(0)=0.890\pm0.005\ .$$

from which we see that $\alpha_c\simeq0.890$. The approximation then has the effect of reducing the critical coupling by $\simeq12\%$ but not of changing the nature of the model. The presence of a chiral phase transition persists even when the kernel is calculated exactly.

It is not difficult to understand why the critical cou-

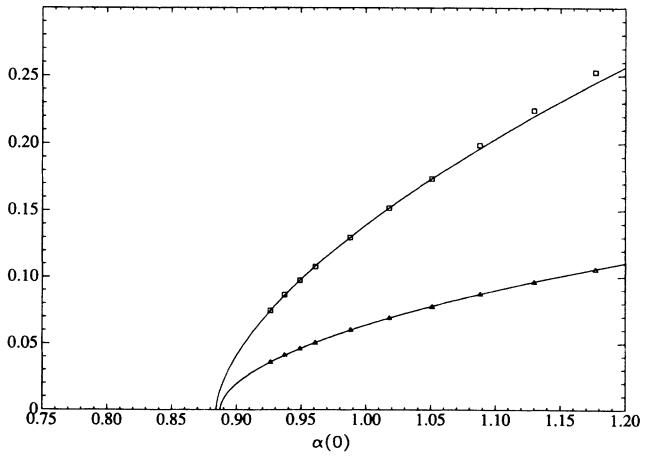

FIG. 6. Same as Fig. 5 but with $N_F=4$.

TABLE II. Parameters obtained in fitting the function in Eq. (3.1) to the data plotted in Figs. 5 and 6 obtained using the exact kernel.

		β	α_c	γ
$N_F=0$	$-\frac{1}{\ln B(0)}$	0.459	0.892	0.567
	$-\frac{1}{\ln\kappa}$	0.178	0.896	0.486
$N_F=4$	$-\frac{1}{\ln B(0)}$	0.519	0.884	0.611
	$-\frac{1}{\ln\kappa}$	0.207	0.887	0.540

pling should be increased when the kernel of the integral equations is treated correctly. Suppose we were to substitute B^{approx}, the solution of the integral equations with the approximated kernel, into the integrand of Eq. (2.2). [We neglect Eq. (2.1) here because $q^2A(q^2)\simeq q^2$ even when the kernels are treated correctly.] In this integrand we have the exact kernel which is uniformly greater than the approximate kernel and so the value of the integral (which was equal to B^{approx} when the approximate kernel was used) is now greater than $B^{\text{approx}}(p^2)$ at each p^2. There are two ways that this can be compensated for in the nonlinear integral equation and B^{exact} found from B^{approx}. In the case where we are approaching the critical coupling B^{approx} is uniformly small and so the nonlinear term $B(q^2)$ in the denominator of the integrand is unimportant for almost all q^2. The integrand can therefore be made smaller by decreasing $B(p^2)$ at all p^2. Clearly, for a given value of $\alpha(0)$, this would lead to $B^{\text{exact}}(p^2)<B^{\text{approx}}(p^2)$ at all p^2. Hence, one expects that as $\alpha(0)$ is decreased B^{exact} will become identically zero before B^{approx} which corresponds to an upward shift in the critical coupling when the exact kernel is used.

The alternative to this scenario is only important when one considers $\alpha(0)\rightarrow\infty$. In this case $B(q^2)$ is uniformly large and the nonlinear term dominates in the integrand for a large range of q^2. The integrand is then made smaller by uniformly increasing $B(p^2)$ which yields a solution of the exact integral equations in which $B^{\text{exact}}>B^{\text{approx}}$ at all p^2. This situation is discussed elsewhere.[12]

IV. SUMMARY AND CONCLUSIONS

We have shown in Sec. II that the often used approximate kernel for the Schwinger-Dyson equation badly misrepresents the true kernel for $p\simeq q$. This approximation underestimates the strength of the coupling for $p\simeq q$ and the discrepancy becomes worse as $\alpha(0)$ is increased. This presents a severe problem in realistic models of QCD with some sort of confinement mechanism included through a very strong (perhaps infinite) coupling at zero momentum transfer. The approximation dramatically changes the effective coupling having the effect of suppressing the confining part of the gluon propagator. Conclusions based on results obtained from the approximate equation are therefore likely to be incorrect, certainly insofar as they are used to constrain the gluonic sector of QCD; for example, one would anticipate that a larger than necessary ratio of the confinement parameter to Λ_{QCD} would be required in spectrum analyses when the approximation is used.

In the present investigation, however, we are in the regime where the approximation does not represent the true situation so poorly. In our investigation of the restoration of chiral symmetry we have studied the limit $\alpha(0)\rightarrow 0$ and, as we have remarked, the discrepancy is not so severe in this regime. This explains why the actual value of the critical coupling $\alpha_c(0)=0.890$ is only 12% greater than that obtained when the phenomenon is investigated using the approximate kernel. Qualitatively, the approximation leads one to the same conclusion as the exact calculation: that there is a minimum value of the running coupling at zero momentum transfer in the QCD model below which chiral symmetry is manifest and the spectrum is completely different to what is observed empirically.

In the context of exact QCD we believe our calculations demonstrate that the existence of DCSB is intimately related to the form of the running coupling constant near $-q^2/\Lambda^2\simeq 0$. They suggest that one does not necessarily need to have confinement (in the sense that the running coupling is infinite at zero momentum transfer) to have DCSB but only a strong $[\alpha_s(0)\sim 1000\times\alpha_{\text{em}}]$ coupling theory. This observation suggests that the deconfinement and chiral-symmetry phase transitions in QCD need not necessarily occur at the same coupling.

Our final remark in closing is simply a note of caution. Approximating the kernel in the Schwinger-Dyson equation provides a computational simplification that *may* lead to qualitatively correct results. We believe, however, that the results presented herein demonstrate that the approximation should not be employed for the purpose of a *quantitative* analysis of any phenomenon.

ACKNOWLEDGMENTS

This work was supported by the Australian Research Grants Committee.

*Present address: Nuclear Theory Group, B203, Argonne National Laboratory, 9700 South Cass Avenue, Argonne, IL 60439.

[1]Kiyoshi Higashijima, Phys. Rev. D **29**, 1228 (1983).

[2]C. D. Roberts, Ph.D. thesis, Flinders University of South Australia, 1987.

[3]J. L. Richardson, Phys. Lett. **82B**, 272 (1979).

[4]G. Krein, P. Tang, and A. G. Williams, Phys. Lett. B **215**, 145 (1988).

[5]C. D. Roberts, R. T. Cahill, and J. Praschifka, Ann. Phys. (N.Y.) **188**, 20 (1988).

[6]D. Atkinson and P. W. Johnson, Phys. Rev. D **37**, 2296 (1988).

[7]See also K. Stam, Phys. Lett. **152B**, 238 (1985); Joseph Otu and K. S. Viswanathan, Phys. Rev. D **34**, 3920 (1986); A. Barduc-

ci *et al.*, *ibid.* **38**, 238 (1988).

[8]For example, T. Appelquist, D. Carrier, L. C. R. Wijewardhana, and W. Zheng, Phys. Rev. Lett. **60**, 1114 (1988); Thomas Appelquist, Kenneth Lane, and Uma Mahanta, *ibid.* **61**, 1553 (1988); Andrew Cohen and Howard Georgi, Nucl. Phys. **B314**, 7 (1989).

[9]C. D. Roberts and R. T. Cahill, Phys. Rev. D **33**, 1755 (1986).

[10]H. David Politzer, Nucl. Phys. **B117**, 397 (1976).

[11]Our calculations were performed on a CYBER 990 computer and were funded by a grant from The University of Melbourne Computer Services Department.

[12]A. G. Williams, G. Krein, and C. D. Roberts, University of Washington report, 1989 (unpublished).